AIP | Applied Physics Letters

Exchange bias in large three dimensional iron oxide nanocomposites

J. R. Morales, S. Tanju, W. P. Beyermann, and J. E. Garay

Citation: Appl. Phys. Lett. **96**, 013102 (2010); doi: 10.1063/1.3277147
View online: http://dx.doi.org/10.1063/1.3277147
View Table of Contents: http://apl.aip.org/resource/1/APPLAB/v96/i1
Published by the American Institute of Physics.

Exchange bias in large three dimensional iron oxide nanocomposites

J. R. Morales,[1] S. Tanju,[1] W. P. Beyermann,[2] and J. E. Garay[1,a)]
[1]*Department of Mechanical Engineering and Materials Science and Engineering Program, University of California, Riverside, California 92521, USA*
[2]*Department of Physics and Astronomy, University of California, Riverside, California 92521, USA*

(Received 25 June 2009; accepted 2 December 2009; published online 4 January 2010)

A processing method is presented for the production of macroscopic nanocomposites that display antiferromagnetic/ferrimagnetic (AFM/fM) coupling. The technique takes advantage of the metastability of iron oxide phases and the fast densification of nanocrystalline powders. The total processing time is under 500s. It is possible to manipulate the composition of fM and AFM phases with processing temperature. The relatively high density of AFM/fM boundaries produces an exchange bias caused by coupling at the interfaces. The magnitude of the exchange field (H_{ex}) is affected the composition as well as the grain size; the smaller grain size samples have the highest H_{ex}. © *2010 American Institute of Physics*. [doi:10.1063/1.3277147]

Various scientifically interesting and technologically important magnetic properties resulting from nanoscale confinement have been reported. Examples include superparamagnetism in nanopowders,[1] increased energy product (product of the permanent magnetic field and the magnetization) in small scale nanocomposites,[2] and exchange bias in thin films.[3] The vast majority of the nanomaterials explored have been powders and thin films with the latter finding the most applications. Thin films have length scale confinement in one dimension but are large in the other two providing easier integration into devices (relative to powders). Along the same lines, increasing sample dimensionality by introducing length scale confinement to bulk [three dimensional (3D)] magnetic materials would provide further advantages. These 3D materials can provide large property magnitudes, improved mechanical integrity, and easier material manipulation; thus providing a platform for a host of advanced magnetic devices. Possible applications are exchange bias based devices, permanent magnets, and electromagnetic communication devices such as microwave waveguides.

Today, a bottle neck for the implementation of bulk three dimensional architectures is that processing technology cannot deliver the desired microstructural control cost effectively in large nanocrystalline materials. In this letter we report an efficient processing method for bulk magnetic nanocomposites that display interesting magnetic coupling. The strategy is twofold. First, the materials are densified from nanocrystalline powders using an electric current activated pressure assisted (CAPAD) technique that has proven effective in densifying materials quickly while minimizing grain growth thus maintaining the nanostructure. This technique is often called spark plasma sintering in the literature. The processing times can be drastically reduced compared to conventional processing by the dual benefits of an applied pressure and current. Second, the metastability of iron oxide phases is leveraged in order to attain a well distributed and intimate composite of antiferromagnetic/ferrimagnetic (AFM/fM) phases necessary to induce magnetic coupling. The method creates large composites having grain sizes in the nanoscale range with clean AFM/fM interfaces.

Exchange bias has become very important in magnetic sensors such as hard drive read heads. One exchange bias magnetic configuration is caused by intimate contact of AFM and fM phases. The mechanism behind exchange bias is thought to be that the fM spins preferentially align with neighboring AFM spins across an interface, producing an exchange coupling between AFM and fM spins.[3] Because the AFM phase is more difficult to rotate with an applied external field, rotation of exchange coupled fM spins is inhibited (pinned). The result is a magnetic composite with spins that are harder to rotate (AFM property) and possess higher remanence and saturation (fM property).

Exchange bias has been observed in many material systems.[3,4] In this work we report on bulk iron oxide nanocomposites. Iron oxide phases with cubic symmetry (γ-Fe_2O_3, Fe_3O_4) are ferrimagnetic (fM) while the hexagonal phase (α-Fe_2O_3) is antiferromagnetic (AFM). Despite the difference in magnetic ordering, these three structures are closely related, and all are based on the close-packing of the oxygen sublattice. The γ-Fe_2O_3 phase transforms into α-Fe_2O_3 at temperatures over 300 °C.[5] A second phase change occurs above 600 °C due to reduction of α-Fe_2O_3 into Fe_3O_4. Thus by producing materials at different temperatures, it is possible to obtain composites with different concentrations of AFM and fM components.

Commercial (Alfa Aesar) γ-Fe_2O_3 powders with average crystallite diameters of 8 and 40 nm were used. The nanopowders were placed in graphite dies for CAPAD processing. All processing was done in vacuum using dies with 19 mm inner diameters. Details of the processing equipment and procedure are available elsewhere.[6]

The samples were cold-pressed inside the dies to a pressure of 71 MPa and the pressure was removed. Then the pressure was raised at a rate of 35 MPa/min over a period of 180 s until the maximum pressure of 106 MPa was reached. When the maximum pressure was reached, current was raised to achieve a heating rate of ~200 °C/min until the desired hold temperature is reached (650, 675, or 900 °C). The pressure and current were removed at a time of 500 s for all samples. The resulting samples after CAPAD processing will be referred to by the starting powder they are made from

a)Author to whom correspondence should be addressed. Electronic mail: jegaray@engr.ucr.edu.

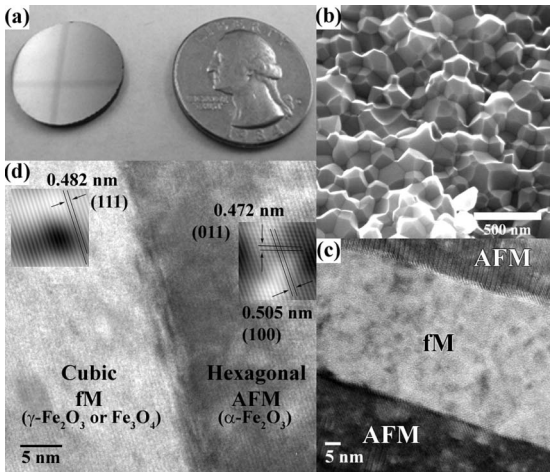

FIG. 1. (a) A picture of a typical iron oxide nanocomposite next to a coin for size reference. (b) SEM micrograph of a 40 nm-675 °C sample, (c) A TEM micrograph of a subgrain region showing a fM phase in between two AFM phases (phases were determined by electron diffraction). (d) TEM micrograph showing a boundary between two different phases in a nanocomposite. The left is a cubic, fM grain (either γ-Fe_2O_3 or Fe_3O_4) while the grain on the right is hexagonal, AFM (α-Fe_2O). The insets are sections that have been enhanced using Fourier filters to enhance the lattice planes.

and their processing temperature. Using this scheme, 8 nm-650 °C and 8 nm-675 °C denote the samples made using 8 nm initial powder and heated to 650 and 675 °C, respectively.

After densification, the microstructure, composition, and magnetic properties of the materials were characterized using scanning electron microscopy (SEM), transmission electron microscopy (TEM), x-ray diffraction (XRD), and field- and temperature-dependent magnetization using a magnetic property measurement system. Sample densities were measured using the Archimedes method with deionized water as a medium. Reported densities are relative to theoretical density and are corrected for sample composition using the law of mixtures in conjunction with XRD composition data. The sample phase composition was measured using a Bruker D8 Advance x-ray diffractometer and freeware software (PowderCell v2.3). Data was collected using Cu-Kα at a 0.04° step size with a 1s/step duration. Average grain size was measured from SEM images taken using a Philips FEG30 (averages of at least 800 measured grains). The densified nanocomposites were characterized magnetically using a SQUID magnetometer (Quantum Design XL7) at various measurement temperatures. The measurements were conducted in a field-cooled environment by heating the samples to 350 K, subjecting them to an applied field of 1 T, and cooling them to the target measuring temperature. H_{ex} is calculated from the positive and negative coercivities (H_c) of horizontally shifted hysteresis curves $[(|-H_c|-H_c)/2]$. Magnetic measurements at each measured temperature were separated by alternating field demagnetization (500 Oe) at 350K.

Figure 1 includes a picture and micrographs of densified iron oxide nanocomposites processed using CAPAD. Figure 1(a) shows a picture of a nanocomposite next to a coin as a size reference, showing these samples are large 3D materials. Figure 1(b) is a representative SEM micrograph of the 40 nm-675 °C sample. Average grain size for 8 nm-650 °C and 8 nm-900 °C samples are 58 and 173 nm. The final grain sizes of the samples processed from 40 nm samples are larger; the 40 nm-675 °C and 40 nm-900 °C have grain sizes of 186 and 558 nm. Thus the grain size of samples are dependent on temperature (higher temperature produced larger grains) and initial powder size (8 nm derived samples had smaller grain sizes than 40 nm derived samples).

The average grain size measured by SEM is very likely an overestimate of the grain size of the materials densified at low temperature (8 nm-650 °C, 40 nm-675 °C). This measurement assumes that the entire grain seen by SEM is either cubic or hexagonal. In reality, it is likely that multiple phases result because of the partial transformation of grains. The TEM micrograph of a sub-grain region shown in Fig. 1(c) reveals that some grains are in fact composed of multiple phases. The phase transformation mechanisms appear to be quite complex and are the subject of ongoing investigations. Grain sizes reported here should serve as a useful upper bound. Figure 1(d) is a TEM micrograph showing an interface (phase boundary) between cubic (fM) and hexagonal (AFM) iron oxide phases.

The processing temperature and initial powder size played a role in sample density. The 8 nm-650 °C had a density of 0.71 while 8 nm-900 °C had a density of 0.94. The 40 nm-675 °C sample had a density of 0.93 while the 40 nm-900 °C is 0.97. Table I summarizes the density, composition, and grain size for the different samples.

XRD analysis revealed that some of the samples are composed of multiple iron oxide phases, i.e., they are composites. Figure 2 shows XRD profiles of 8 nm-650 °C and 40 nm-675 °C samples. Peaks associated with both cubic (γ-Fe_2O_3 or Fe_3O_4) and hexagonal (α-Fe_2O_3) phases are present and identified by the symbols in the profile. As mentioned earlier γ-Fe_2O_3 transforms into α-Fe_2O_3 and α-Fe_2O_3 into Fe_3O_4 at high temperatures. Thus the coexistence of the phases can be attributed to a partial phase transformation at the processing temperatures. The similarities in the relative peak heights for the XRD profiles in Fig. 2 suggest that the samples have a very similar phase composition. A quantitative analysis of the XRD profiles confirms that the 8

TABLE I. A summary of the properties and physical characteristics of the nanocomposites. AFM refers antiferromagnetic (α-Fe_2O_3) phase and fM to ferrimagnetic phases (γ-Fe_2O_3 or Fe_3O_4).

Sample	Composition AFM (%)	Composition fM (%)	Relative density	SEM grain size (nm)	Coercivity @ maximum H_{ex} (Oe)	Maximum exchange field, H_{ex} (Oe)
8 nm-650 °C	80.3	19.7	0.71	58	583	63
40 nm-675 °C	80.7	19.3	0.94	186	178	26
8 nm-900 °C	0	100	0.93	173	212	6
40 nm-900 °C	0	100	0.97	558	35	3

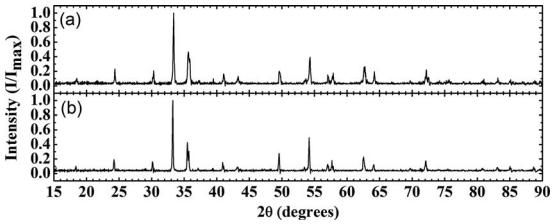

FIG. 2. XRD profiles of (a) 8 nm-650 °C sample and (b) 40 nm-675 °C sample. The peaks are due to cubic (γ-Fe_2O_3 or Fe_3O_4) and hexagonal (α-Fe_2O_3) phases.

nm-650 °C sample is composed of 19.7% α-Fe_2O_3 with the remainder a cubic phase. The 40 nm-675 °C sample has a nearly identical composition (19.3% α-Fe_2O_3 with the remainder being cubic phase). XRD profiles of both 8 nm-900 °C and 40 nm-900 °C samples (not shown here) show only cubic peaks. The similarities in phase composition of both the low temperature (650 or 675 °C) and high temperature (900 °C) samples will be important later when we compare the magnetic properties.

Because the nanocomposites have both AFM and fM phases (Fig. 2) with well defined interfaces [Fig. 1(d)] it is possible that they display an exchange bias. Indeed, magnetic hysteresis measurements of some samples revealed shifted hysteresis loops. Fig. 3 is a plot of the exchange field for the samples produced at different temperatures versus measurement temperature. Inspection of the plot shows that the initial powder size, processing temperature, and measurement temperature play a role in the magnitude of H_{ex}. The samples processed at low temperatures show significant exchange fields at all temperatures measured. The 8 nm-650 °C had the highest exchange fields. The existence of exchange fields in these samples strongly suggests that there is AFM/fM coupling at the interfaces. Both 8 nm-650 °C and 40 nm-675 °C show drops in H_{ex} at ~80 and 120 K, respectively. H_{ex} for these two samples appears to increase at 220 K, with the 8 nm-650 °C sample showing a steeper increase. H_{ex} does not exceed 6 Oe for either the 8 nm-900 °C or 40 nm-900 °C samples.

It is not surprising that the materials processed at 900 °C do not display significant shifts (H_{ex}) since the AFM phase is absent in their XRD profiles. This finding highlights the importance of the proper processing temperature. Fig. 3 also reveals that although the 8 nm-650 °C and 40 nm-675 °C materials have practically the same composition, they have significantly different H_{ex}. We believe that the exchange bias magnitudes in this case are influenced by grain sizes. A likely explanation is that because the 8 nm derived samples have a significantly smaller grain size, they have a higher concentration of interfaces producing a higher overall exchange field.

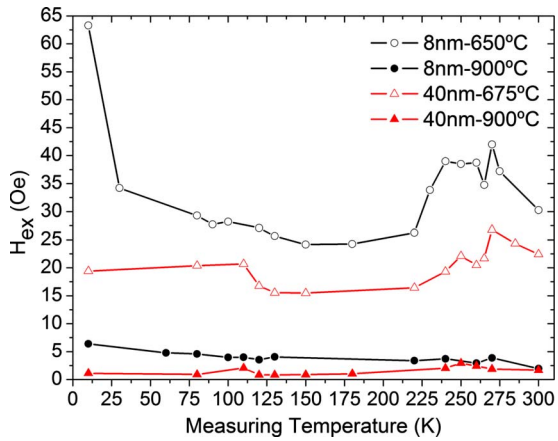

FIG. 3. (Color online) A plot of the exchange field for several samples produced at different temperatures vs measurement temperature. The magnitude of H_{ex} depends on phase composition and grain size.

The temperature dependence of H_{ex} is interesting as well. The materials produced at low temperatures display a low-temperature maximum and a second maximum near room temperature. It is typical for the exchange field to decrease with increasing measurement temperature because the excess thermal energy decreases the strength of the pinning.[7] This explains the lower H_{ex} found at increasing measurement temperature (relative to 10 K). It is more difficult to understand the increase in H_{ex} that occurs around room temperature. This behavior may be associated with spin reorganization at the Morin transition of α-Fe_2O_3 (Refs. 5 and 8) that occurs at ~260–180 K, depending on grain size. While the exact mechanism for influence on H_{ex} is not known, the new spin arrangement caused by the Morin transition might increase the AFM/fM coupling. Recent experiments have shown that the bulk AFM moments play a role in exchange bias.[9]

Exchange bias has been observed in iron oxide systems before, but in powder form.[3] More commonly, exchange bias is associated with technologically important thin films. Many thin film materials have significantly higher H_{ex} than those reported here at low temperatures. However, the exchange fields are comparable to some advanced thin film materials at near room temperature.[10] In summary we have shown that starting with γ-Fe_2O_3 iron oxide nanocrystalline powder one can obtain large 3D nanocomposites using the CAPAD technique. The composition of the materials depends on the processing temperature, while the final grain size depends on both the processing temperature and the initial starting powder size. The composites produced at lower temperature display exchange bias. The magnitude of the exchange field appears to be grain size dependent as well.

This work is dedicated to the memory of our friend Dr. Maurizio Biasini. Support from the AFOSR through a Young Investigator Program is most gratefully acknowledged. We also appreciate support from ONR/DMEA through the Center of Nanomaterials and Nanodevices (CNN) under the Award No. H94003-08-2-0803. We thank C. Vance for help with SEM grain size measurements.

[1]S. Maenosono, T. Suzuki, and S. Saita, J. Magn. Magn. Mater. **320**, L79 (2008).
[2]H. Zeng, J. Li, J. P. Liu, Z. L. Wang, and S. Sun, Nature (London) **420**, 395 (2002).
[3]J. Nogues and K. Ivan Schuller, J. Magn. Magn. Mater. **192**, 203 (1999).
[4]P. J. van der Zaag, R. M. Wolf, A. R. Ball, C. Bordel, L. F. Feiner, and R. Jungblut, J. Magn. Magn. Mater. **148**, 346 (1995).
[5]U. Schwertmann and R. M. Cornell, *The Iron Oxides: Structure, Properties, Occurrences, and Uses*, 2nd ed. (VCH, Weinheim, 1991).
[6]S. R. Casolco, J. Xu, and J. E. Garay, Scr. Mater. **58**, 516 (2008).
[7]U. Nowak and K. D. Usadel, Phys. Rev. B **66**, 014430 (2002).
[8]E. Fritzsch, C. Pietzsch, H. Heegn, and H. J. Huhn, Cryst. Res. Technol. **17**, 1443 (1982).
[9]R. Morales, Z.-P. Li, J. Olamit, K. Liu, J. M. Alameda, and I. K. Schuller, Phys. Rev. Lett. **102**, 097201 (2009).
[10]J. I. Hong, T. Leo, D. J. Smith, and A. E. Berkowitz, Phys. Rev. Lett. **96**, 117204 (2006).